

A Flexible Phase Retrieval Framework for Flux-limited Coherent X-Ray Imaging

Liang Shi and Gordon Wetzstein

Department of Electrical Engineering, Stanford University, Stanford, California 94305, USA

Thomas J. Lane*

*SLAC National Accelerator Laboratory, Menlo Park, California 94025, USA**

(Dated: July 29, 2022)

Coherent X-ray diffraction imaging (CXDI) experiments are intrinsically limited by shot noise, a lack of prior knowledge about the sample’s support, and missing measurements due to the experimental geometry. We propose a flexible, iterative phase retrieval framework that allows for accurate modeling of Gaussian or Poissonian noise statistics, modified support updates, regularization of reconstructed signals, and handling of missing data in the observations. The proposed method is efficiently solved using alternating direction method of multipliers (ADMM) and is demonstrated to consistently outperform state-of-the-art algorithms for low-photon phase retrieval from CXDI experiments, both for simulated diffraction patterns and for experimental measurements.

Propelled by the development of ultra-bright 4th generation light sources like the linac coherent light source (LCLS), coherent X-ray diffraction imaging (CXDI) has the promise of revealing the atomic or near-atomic structure of aperiodic structures like single, non-crystalline proteins [1–4].

In a common implementation of such experiments, identically-structured particles are exposed to coherent X-ray pulses at unknown orientations and a detector records the intensity of forward-scattered diffraction patterns. Real-space images can then be retrieved by means of iterative phase retrieval algorithms [5–9], for example the hybrid input-output (HIO) and relaxed averaged alternating reflections (RAAR).

To employ any of these algorithms, it is necessary to “oversample” the diffraction patterns by a factor of at least 2x (in the Shannon sense) [10]. Due to this oversampling, reconstructed molecules only occupy part of the image, known as the *support*. Unfortunately, the specific support of any sample is usually unknown and has to be estimated. For example, the Shrinkwrap algorithm [2], one of the most common approaches, thresholds the real-space image at each iteration to provide a continuously updated support estimate. An accurate support is crucial for reliable reconstructions.

A second unavoidable challenge in phase retrieval is Poisson-distributed shot noise due to the fact that source brightness or radiation damage intrinsically limits the number of photons a given sample can diffract [11]. The resolution at which an image can be inferred is directly limited by the total number of photons diffracted [12]. Most iterative phase retrieval algorithms implicitly assume and work under a Gaussian noise model, which is not optimal for low-photon imaging. This model mismatch is negligible when many photons are captured by each camera pixel ($\gg 10$), but it becomes significant when photons are scarce.

Finally, in most CXDI experiments, the direct beam necessitates a beam dump or stop to prevent damage

to experimental equipment, resulting in a missing region in the center of the detector that corresponds to low frequency information. This missing information can severely limit the quality of a reconstruction or make it impossible [3, 13–15]. Since missing frequencies are unconstrained by available experimental data, they often remain near the random initial values set by the phase retrieval method employed, resulting in significant artifacts in the reconstructed image. A common empirical solution is to fix the missing intensities to physically motivated values (see *e.g.* [3]). A recent study [16], however, demonstrated that prior information about the real space image, such as total variation regularization (TV) [17], could sufficiently constrain missing intensities, resulting in reproducible, high-quality reconstructions. However, the regularization was carried out in an *ad hoc* manner separate from the phase retrieval algorithm employed (HIO) and therefore was not easily interfaced with other methods.

In this letter, we propose a framework for combining different prior information in an efficient and flexible way leveraging the alternating direction method of multipliers (ADMM) [18], which has been shown success in phase retrieval for sparse signals [19, 20]. Within this framework, we implement a Poisson error model, TV regularization, support update model, and handle missing measurements in a unified manner. Our method is compatible with classic update rules like HIO and RAAR.

To be precise, we introduce a notation for CXDI measurements and quickly review these classic phase retrieval algorithms before describing our method mathematically. Let \mathbf{x} be a finite scalar field representing the electron density of an object, generally in 3 dimensions (though our results also apply to physically interesting cases of 2D objects, or 2D manifolds within a 3D object). We will employ a vectorized representation $\mathbf{x} \in \mathbb{R}^N$, where x_i denotes a voxel value at index i , and i runs over all voxels in all dimensions. In CXDI, we measure the diffraction

image

$$\mathbf{b} = |\mathcal{F}\mathbf{x}|^2, \quad (1)$$

where $\mathbf{b} \in \mathbb{R}^N$ is the measured Fourier intensity and \mathcal{F} is the 3D discrete Fourier transform operator. Let \mathbf{S}^k be the *support*, that is $x_i = 0$ if $i \notin \mathbf{S}^k$, at iteration k . Define projection operator $\mathbf{P}_{\mathbf{m}}$,

$$\mathbf{P}_{\mathbf{m}}(\mathbf{x}) = \mathcal{F}^{-1}(\mathbf{v}), \quad v_i = \begin{cases} b_i \frac{(\mathcal{F}\mathbf{x})_i}{|(\mathcal{F}\mathbf{x})_i|} & \text{if } (\mathcal{F}\mathbf{x})_i \neq 0 \\ (\mathcal{F}\mathbf{x})_i & \text{otherwise} \end{cases} \quad (2)$$

which projects a current estimate of the object image onto the set of images consistent with the measured diffraction image.

The three classic algorithms we consider consist of iterative updates, where in-support pixels are updated according to

$$x_i^{k+1} = (\mathbf{P}_{\mathbf{m}}\mathbf{x}^k)_i, \quad i \in \mathbf{S}^k, \quad (3)$$

and out-of-support pixels are updated by one of (where the algorithm is indicated)

$$x_i^{k+1} = \begin{cases} 0 & ER \\ x_i^k - \beta(\mathbf{P}_{\mathbf{m}}\mathbf{x}^k)_i & HIO, i \notin \mathbf{S}^k. \\ \beta x_i^k + (1 - 2\beta)(\mathbf{P}_{\mathbf{m}}\mathbf{x}^k)_i & RAAR \end{cases} \quad (4)$$

with β a parameter (a typical value of β is 0.9). The update rule for pixels inside the support can be interpreted as a gradient descent update which minimizes

$$\varepsilon_m = \|\mathcal{F}\mathbf{x} - \sqrt{\mathbf{b}}\|_2^2, \quad (5)$$

followed by projection onto the feasible set in real space, i.e. support \mathbf{S}^k [9].

The model above assumes the diffracted wavefront can be measured perfectly. A real experiment is better modeled by a Poisson process that takes into account photon shot statistics

$$\mathbf{b} \sim \mathcal{P}(|\mathcal{F}\mathbf{x}|^2). \quad (6)$$

specifically, the probability of observing b_i photons at pixel i is

$$p(b_i|\mathbf{x}) = \frac{(|\mathcal{F}\mathbf{x}|^2)_i^{b_i} e^{-(|\mathcal{F}\mathbf{x}|^2)_i}}{b_i!} \quad (7)$$

to conveniently deal with missing regions (due to e.g. the beam stop), we introduce $\mathbf{W} \in \mathbb{R}^N$, a binary vector with value 0 for pixels in missing regions and 1 otherwise. The log-likelihood of the joint probability can then be expressed in following compact form

$$L_{\mathbf{W}}(\mathbf{x}) = (\text{diag}(\mathbf{W})\log(|\mathcal{F}\mathbf{x}|^2))^T \mathbf{b} - (\text{diag}(\mathbf{W})|\mathcal{F}\mathbf{x}|^2)^T \mathbf{1} - \sum_{i=1}^N W_i \log(b_i!), \quad (8)$$

with gradient

$$\nabla L_{\mathbf{W}}(\mathbf{x}) = 2\mathcal{F}^{-1} \left(\mathcal{F}\mathbf{x} - \text{diag}(\mathbf{W}) \left(\text{diag}(|\mathcal{F}\mathbf{x}|^2)^{-1} \text{diag}(\mathcal{F}\mathbf{x})\mathbf{b} \right) \right) \quad (9)$$

allowing the log-likelihood to be efficiently maximized by gradient ascent. This gradient demonstrates the natural first approach to missing intensities is to not modify their values.

We add two pieces of prior knowledge to this model of the measurement: that we expect the resulting image to be smooth and positive. This is not an exhaustive list of prior information that could be employed, but will be used to demonstrate the power of our approach. We add prior terms directly to the objective function, allowing for continuous enforcement of this information. No intensity constraints are applied to missing-measurement regions, though these regions are implicitly constrained by our real-space priors. Our phase retrieval problem can then be stated,

$$\underset{\mathbf{x}}{\text{minimize}} \quad -\log(p_{\mathbf{W}}(\mathbf{b}|\mathbf{x})) + \lambda \|\mathbf{D}\mathbf{x}\|_1 + \mathcal{I}_{\mathbb{R}_+}(\mathbf{x}), \quad (10)$$

where \mathbf{D} is a gradient operator, λ is the weight for the isotropic TV term and $\mathcal{I}_{\mathbb{R}_+}(\mathbf{x})$ is the indicator function

$$\mathcal{I}_{\mathbb{R}_+}(\mathbf{x}) = \begin{cases} 0 & x_i \in \mathbb{R}_+ \\ +\infty & x_i \notin \mathbb{R}_+ \end{cases}, \quad (11)$$

enforcing positivity.

This problem can be efficiently solved by the alternating direction of multiplier methods (ADMM) [18]. Using ADMM, Eq. (10) is reformulated as

$$\underset{\mathbf{x}}{\text{minimize}} \quad \underbrace{-\log(p_{\mathbf{W}}(\mathbf{b}|\mathbf{x}))}_{f(\mathbf{x})} + \lambda \underbrace{\|\mathbf{z}_1\|_1}_{g_1(\mathbf{z}_1)} + \underbrace{\mathcal{I}_{\mathbb{R}_+}(\mathbf{z}_2)}_{g_2(\mathbf{z}_2)} \quad (12)$$

$$\text{subject to} \quad \underbrace{\begin{bmatrix} \mathbf{D} \\ \mathbf{I} \end{bmatrix}}_{\mathbf{K}} \mathbf{x} - \underbrace{\begin{bmatrix} \mathbf{z}_1 \\ \mathbf{z}_2 \end{bmatrix}}_{\mathbf{z}} = 0, \quad (13)$$

where $\mathbf{z}_1 \in \mathbb{R}^{2N}$ and $\mathbf{z}_2 \in \mathbb{R}^N$ are slack variables. ADMM splits the objective into a weighted sum of three independent functions $f(\mathbf{x})$, $g_1(\mathbf{z}_1)$ and $g_2(\mathbf{z}_2)$ that are only linked through the stated constraints. Following the general ADMM strategy, we write an augmented Lagrangian of Eq. (12)

$$L_{\rho_1, \rho_2}(\mathbf{x}, \mathbf{z}, \mathbf{y}) = f(\mathbf{x}) + g_1(\mathbf{z}_1) + g_2(\mathbf{z}_2) + \mathbf{y}^T (\mathbf{K}\mathbf{x} - \mathbf{z}) + \frac{\rho_1}{2} \|\mathbf{D}\mathbf{x} - \mathbf{z}_1\|_2^2 + \frac{\rho_2}{2} \|\mathbf{x} - \mathbf{z}_2\|_2^2, \quad (14)$$

where ρ_1 and ρ_2 set control the penalty associated with violating the ADMM constraints. Using the scaled form of the augmented Lagrangian, the following iterative

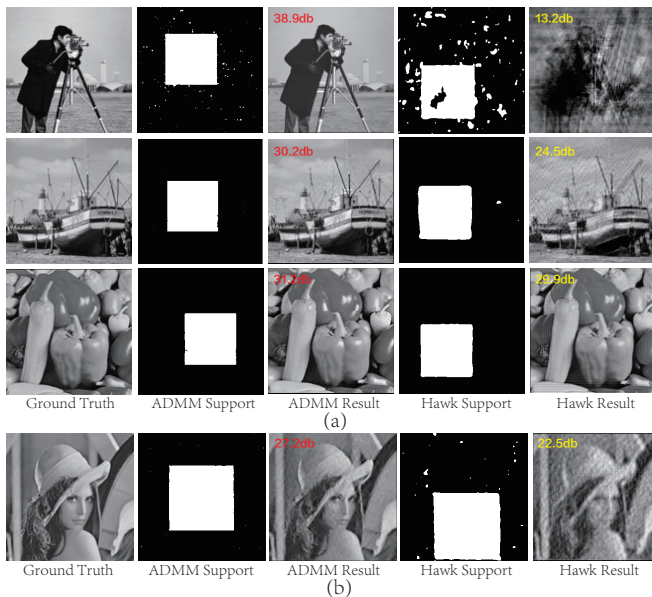


FIG. 1. (a, top 3 rows) Reconstructed “Cameraman”, “Boat”, “Peppers” and associated supports from 2.5x oversampled noise-free simulations. (b, bottom row) Reconstructed “Lena” and support from 2x oversampled Poisson-noise simulations with an average 150 photons/px. PSNRs indicated on top-left corner of each image.

updates rules can be derived:

$$\begin{aligned}
 \mathbf{x} &\leftarrow \mathbf{prox}_{quad, \rho_1, \rho_2}(\mathbf{v}_1, \mathbf{v}_2) = \\
 &\arg \min_{\mathbf{x}} f(\mathbf{x}) + \frac{\rho_1}{2} \|\mathbf{D}\mathbf{x} - \mathbf{v}_1\|_2^2 \\
 &\quad + \frac{\rho_2}{2} \|\mathbf{x} - \mathbf{v}_2\|_2^2, \quad \mathbf{v}_1 = \mathbf{z}_1 - \mathbf{u}_1, \quad \mathbf{v}_2 = \mathbf{z}_2 - \mathbf{u}_2 \\
 \mathbf{z}_1 &\leftarrow \mathbf{prox}_{\|\cdot\|_1, \rho_1}(\mathbf{v}) = \arg \min_{\mathbf{z}_1} g_1(\mathbf{z}_1) + \frac{\rho_1}{2} \|\mathbf{v} - \mathbf{z}_1\|_2^2, \\
 \mathbf{v} &= \mathbf{D}\mathbf{x} + \mathbf{u}_1 \\
 \mathbf{z}_2 &\leftarrow \mathbf{prox}_{\mathcal{I}, \rho_2}(\mathbf{v}) = \arg \min_{\mathbf{z}_2} g_2(\mathbf{z}_2) + \frac{\rho_2}{2} \|\mathbf{v} - \mathbf{z}_2\|_2^2, \\
 \mathbf{v} &= \mathbf{x} + \mathbf{u}_2 \\
 \underbrace{\begin{bmatrix} \mathbf{u}_1 \\ \mathbf{u}_2 \end{bmatrix}}_{\mathbf{u}} &\leftarrow \mathbf{u} + \mathbf{K}\mathbf{x} - \mathbf{z},
 \end{aligned}$$

where the scaled dual variable $\mathbf{u} = (1/\rho)\mathbf{y}$ is used to simplify the notation of Eq. (14).

The \mathbf{x} -update is a quadratic program which can be iteratively solved by gradient-based methods. Upon completion, out-of-support pixels can be updated using rules defined by HIO or RAAR.

After t ADMM iterations, we update the object support using a modified Shrinkwrap algorithm, which we describe next. Let $G(k_r)$ be a normalized Gaussian blurring kernel with standard deviation k_r , and η be a thresholding parameter. Traditional Shrinkwrap updates the

support by convolving the realspace image with a Gaussian and thresholding, precisely

1. $\mathbf{x}_g = |\mathbf{x}| * G(k_r)$
2. $\mathbf{S} = \{i \mid (\mathbf{x}_g)_i \geq \eta \max(\mathbf{x}_g)\}$.

Inspired by recent study which showed that overestimating the extent of the support results in significantly less error than underestimating it[15], we added a third step that fills in any non-support regions completely enclosed by the support. We also experimented with including the entire convex hull of the Shrinkwrap support, with good but inferior results.

For the \mathbf{z}_1 and \mathbf{z}_2 update steps, closed-form solutions can be obtained using proximate operators for the ℓ_1 -norm and indicator function, as discussed in [21].

The ADMM framework offers several advantages, enabling flexible expression of models that can be coded quickly and solved quickly. For example, our model is still compatible with a Gaussian error model, only the cost function of the \mathbf{x} -update and its gradient need to be changed. Because the slack variable (\mathbf{z}) update is separated from the unknown variable (\mathbf{x}) update, changing or imposing new priors is convenient, as one may add a new update rule by simply adding a quadratic term to the \mathbf{x} -update and adding a new slack variable update rule. This modular aspect of ADMM is extremely appealing for phase retrieval applications, where different imaged objects will warrant flexible priors, and it may be desirable to attempt many reconstruction methods to achieve the best result.

To assess the proposed algorithm, we apply it to both simulated diffraction patterns and experimental measurement imaged at LCLS. The results are compared with the ones produced by the state-of-the-art phase retrieval toolbox Hawk [22].

We start with standard test images. Each image was resized to 128×128 px and zero-padded to 320×320 px, resulting in a 2.5x oversampled diffraction pattern after Fourier transformation. The initial support was obtained by thresholding the inverse Fourier transform of intensity measurement (autocorrelation) at 4% of the maximum. The width of the shrinkwrap Gaussian kernel was initialized to $\sigma = 3$ and reduced by 1% every 20 iterations down to a minimum of $\sigma = 1.5$. The parameters $\eta = [5\%, 10\%, 15\%, 20\%]$ and $\lambda = [0.01, 0.005, 0.002, 0.001]$ were tested and the resulting highest peak signal-to-noise ratio (PSNR) reconstruction was chosen. The slack variable ρ_1 was set to $50\lambda / \max(\mathbf{x})$ and $\rho_2 = \rho_1/100$. For the proposed algorithm, the Gaussian model was used for noise-free simulations and the Poisson model was used for simulated noisy measurements that sampled from the original with Poisson statistics. We ran 2000 HIO iterations with $\beta = 0.9$ for both Hawk and our ADMM algorithm, where the last 50 iterations of our algorithm is switched to ER update for a clean out-of-support background.

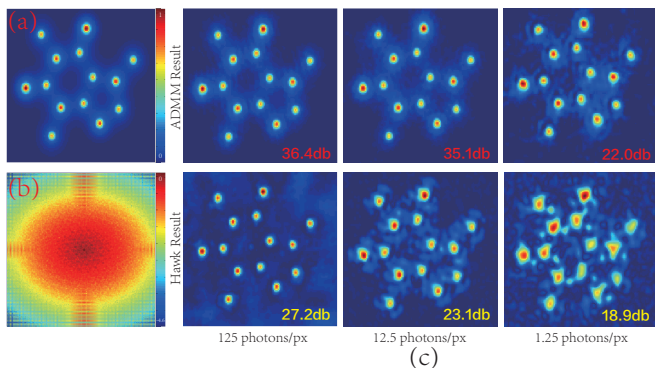


FIG. 2. (a, leftmost column, top) 2D electron density of caffeine molecule and (b, bottom) associated diffraction image with \log_{10} scaling. (c, rightmost columns) Reconstructed caffeine molecule from 2x oversampled shot-noise simulations, sampled from the original image (b) with Poisson statistics at average [125, 12.5, 1.25] photons/px, (top) ADMM HIO and (bottom) Hawk HIO.

Fig. 1a shows the reconstructed supports and images from both algorithms. The failure of Hawk HIO on the “Cameraman” reconstruction demonstrates the importance of support estimation. The low pixel values of the camera man’s black coat produce holes in the support estimated by the Hawk, whereas our modified Shrinkwrap fills these in, leading to a faithful reconstruction. Results of the “Boat” and “Peppers” scenes show how TV regularization alleviates noise and artifacts. The “Boat” contains many fine-grained details and Hawk HIO yields a noisy reconstruction even when the estimated support is approximately correct. Similarly, “Peppers” reconstructed by Hawk HIO is contaminated with grid artifacts. In comparison, ADMM HIO produces less noisy results and more accurate supports with sharper borders.

Fig. 1b shows the reconstructed “Lena” scene and support from simulated measurements exhibiting Poisson noise. The model mismatch of Hawk HIO results a noisy and detail-blurred “Lena”, whereas the ADMM HIO produces a more faithful “Lena”.

For a more experimentally relevant test, we simulated diffraction patterns from a caffeine molecule’s electron density [23]. Fig. 2 shows the reconstructed results from measurements at different noise levels. At lower photon levels, Hawk increasingly suffers from blob artifacts, where ADMM HIO can consistently reconstruct a meaningful image even with 10 times fewer photons. Further, we observed faster convergence and less fluctuation during iterations with the ADMM HIO method.

Finally, we assess the proposed algorithm on experimentally measured mimivirus diffraction patterns obtained at LCLS. Data were obtained from the Coherent X-ray Imaging Data Bank[24]. The 512×512 px measurement contains a missing-measurement sphere of radius 35 px and a 20 px tall horizontal missing-measurement

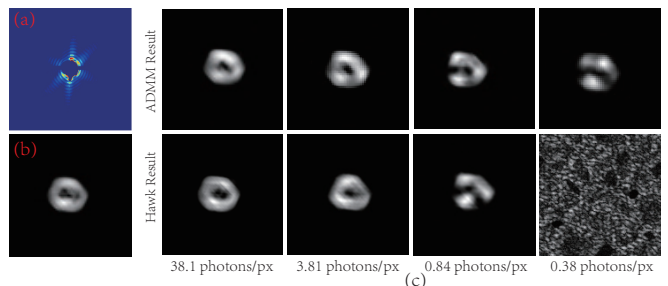


FIG. 3. (top left) Experimentally recorded far-field diffraction pattern of a single mimivirus. (top right) Reconstructed mimivirus from the original measurement using Hawk’s implementation of RAAR. (last 4 columns) Reconstructed mimivirus from Poisson-noised measurement at average [38.1, 3.81, 0.84, 0.38] photons/px, using both (top) ADMM RAAR and (bottom) Hawk RAAR.

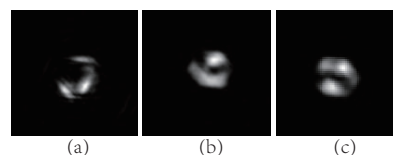


FIG. 4. Reconstructed mimivirus from Poisson-noised measurement at average 0.38 photons/px using different ADMM RAAR settings. (a, left) Gaussian error model + standard Shrinkwrap. (b, center) Poisson error model + standard Shrinkwrap. (c, right) Poisson error model + modified Shrinkwrap

slit at the center. The RAAR algorithm was applied to enable comparison to published results [4]. We employed the area-based Shrinkwrap algorithm and RAAR parameters used to reconstruct the mimivirus in that work.

Fig. 3 shows the reconstructed mimivirus from simulations at different noise levels, where we modeled the original measurement as noise-free ground-truth and sampled it with Poisson statistics to mimic the diffraction from a smaller object or weaker source. For Hawk RAAR, a dramatic drop in reconstruction quality occurs at 0.84 photons/px, and the virus becomes completely irretrievable at 0.38 photons/px. Instead, ADMM RAAR preserves the approximate shape of virus at 0.38 photons/px, with one missing and one attenuated edge of the hexagon. Fig. 4 shows how the Poisson model and the modified Shrinkwrap algorithm play important roles in a successful reconstruction.

In conclusion, we propose a flexible and practical phase retrieval framework incorporating Poisson noise statistics, missing observations, sparse regularization of the reconstructed data, and modified support updates. It is efficiently solved using ADMM and can be easily extended with additional priors. The proposed algorithm produces high-quality reconstructions, in particular for CXDI measurements with low photon counts.

This work was funded through the Linac Coherent

Light Source Directorate (LCLS), SLAC National Accelerator Laboratory, supported by the U.S. Department of Energy, Office of Science, Office of Basic Energy Sciences under Contract No. DE-AC02-76SF00515. We would also like to thank Daniel Ratner for comments on a draft.

* tjlane@slac.stanford.edu

- [1] J. Miao, P. Charalambous, J. Kirz, and D. Sayre, *Nature* **400**, 342 (1999).
- [2] S. Marchesini, H. He, H. N. Chapman, S. P. Hau-Riege, A. Noy, M. R. Howells, U. Weierstall, and J. C. H. Spence, *Phys. Rev. B* **68**, 140101 (2003).
- [3] P. Thibault, V. Elser, C. Jacobsen, D. Shapiro, and D. Sayre, *Acta Crystallographica Section A: Foundations of Crystallography* **62**, 248 (2006).
- [4] M. M. Seibert, T. Ekeberg, F. R. Maia, M. Svenda, J. Andreasson, O. Jönsson, D. Odić, B. Iwan, A. Rocker, D. Westphal, *et al.*, *Nature* **470**, 78 (2011).
- [5] R. W. Gerchberg and W. O. Saxton, *Optik (Stuttgart)* **35** (1972).
- [6] J. R. Fienup, *Appl. Opt.* **21**, 2758 (1982).
- [7] H. H. Bauschke, P. L. Combettes, and D. R. Luke, *J. Opt. Soc. Am. A* **20**, 1025 (2003).
- [8] D. R. Luke, *Inverse Problems* **21**, 37 (2005).
- [9] S. Marchesini, *Review of scientific instruments* **78**, 011301 (2007).
- [10] D. Sayre, *Acta Crystallographica* **5**, 843 (1952).
- [11] S. Ikeda and H. Kono, *Opt. Express* **20**, 3375 (2012).
- [12] A. Aquila, A. Barty, C. Bostedt, S. Boutet, G. Carini, P. Drell, S. Doniach, K. Downing, T. Earnest, H. Elmlund, *et al.*, *Structural Dynamics* **2**, 041701 (2015).
- [13] Y. Nishino, J. Miao, and T. Ishikawa, *Phys. Rev. B* **68**, 220101 (2003).
- [14] J. Miao, Y. Nishino, Y. Kohmura, B. Johnson, C. Song, S. H. Risbud, and T. Ishikawa, *Phys. Rev. Lett.* **95**, 085503 (2005).
- [15] X. Huang, J. Nelson, J. Steinbrener, J. Kirz, J. J. Turner, and C. Jacobsen, *Opt. Express* **18**, 26441 (2010).
- [16] K. He, M. K. Sharma, and O. Cossairt, *Opt. Express* **23**, 30904 (2015).
- [17] L. I. Rudin, S. Osher, and E. Fatemi, *Physica D: Non-linear Phenomena* **60**, 259 (1992).
- [18] S. Boyd, N. Parikh, E. Chu, B. Peleato, and J. Eckstein, *Foundations and Trends® in Machine Learning* **3**, 1 (2011).
- [19] P. Netrapalli, P. Jain, and S. Sanghavi, *Signal Processing, IEEE Transactions on* **63**, 4814 (2015).
- [20] D. S. Weller, A. Pnueli, G. Divon, O. Radzyner, Y. C. Eldar, and J. A. Fessler, *Computational Imaging, IEEE Transactions on* **1**, 247 (2015).
- [21] N. Parikh and S. P. Boyd, *Foundations and Trends in optimization* **1**, 127 (2014).
- [22] F. R. Maia, T. Ekeberg, D. Van Der Spoel, and J. Hajdu, *Journal of applied crystallography* **43**, 1535 (2010).
- [23] H. M. Berman, T. Battistuz, T. Bhat, W. F. Bluhm, P. E. Bourne, K. Burkhardt, Z. Feng, G. L. Gilliland, L. Iype, S. Jain, *et al.*, *Acta Crystallographica Section D: Biological Crystallography* **58**, 899 (2002).
- [24] F. R. Maia, *Nature methods* **9**, 854 (2012).